Independent Freezing of Charge and Spin Dynamics in $La_{1.5}Sr_{0.5}CoO_4$

I. A. Zaliznyak,[1] J. P. Hill,[1] J. M. Tranquada,[1] R. Erwin,[2] and Y. Moritomo[3]
[1]*Department of Physics, Brookhaven National Laboratory, Upton, New York 11973-5000*
[2]*National Institute of Standards and Technology, Gaithersburg, Maryland 20899*
[3]*Center for Integrated Research in Science and Engineering (CIRSE) and Department of Applied Physics, Nagoya University, Nagoya 464-01, Japan*
(Received 8 June 2000)

We present elastic and quasielastic neutron scattering measurements characterizing peculiar short-range charge-orbital and spin order in the layered perovskite material $La_{1.5}Sr_{0.5}CoO_4$. We find that below $T_c \approx 750$ K holes introduced by Sr doping lose mobility and enter a statically ordered *charge glass* phase with loosely correlated checkerboard arrangement of empty and occupied $d_{3z^2-r^2}$ orbitals (Co^{3+} and Co^{2+}). The dynamics of the resultant mixed spin system is governed by the anisotropic nature of the crystal-field Hamiltonian and the peculiar exchange pattern produced by the orbital order. It undergoes a *spin freezing* transition at a much lower temperature, $T_s \lesssim 30$ K.

PACS numbers: 71.28.+d, 71.45.Lr, 75.40.Gb, 75.50.Ee

The instability of the doped transition-metal oxides towards formation of cooperative charge and spin ordered phases is one of the central phenomena in the physics of colossal magnetoresistance (CMR) materials and high-temperature superconductors. Charge segregation into lines [1] which separate stripes of antiferromagnetic domains in $La_{2-x}Sr_xCuO_{4+y}$ (LSCO) cuprates at small x, is, according to some theories, key to their superconductivity [2]. In perovskite manganates, built of essentially isostructural Mn-O layers, doping first destroys the cooperative Jahn-Teller (JT) distortion of the orbitally ordered insulating state [3,4], and induces a transition to a ferromagnetic metal (FM) [5]. The extremely strong response of transport properties to an applied magnetic field [6], termed CMR, results from the strong Hund's coupling of charge carriers to the Mn^{4+} core spins [7]. At doping $x \approx 0.5$, an instability towards another kind of charge-orbital order, with a checkerboard arrangement of Mn^{3+}/Mn^{4+} ions, results in an antiferromagnetic (AFM) insulating ground state. At half doping, transport properties show the strongest response to a magnetic field [6]. Recent experiments [8,9] suggested that charge/orbital order (CO/OO) in $La_{0.5}Ca_{0.5}MnO_3$ is, in fact, a by-product of the peculiar kind of spin order (SO), balancing the double exchange and superexchange interactions [10]. Whether this behavior is indeed generic for the half-doped compounds (or at least manganites), and what is the relative importance of other interactions (Coulomb repulsion between holes, JT distortion), are topics of continuing debate.

The first complete characterization of the spin and charge order in the half-doped regime by means of neutron diffraction was reported for $La_{1.5}Sr_{0.5}MnO_4$ [11]. Nuclear scattering accompanying the CO was found below $T_c \approx 217$ K, where the steep rise in resistivity manifests the transition to an insulating state. A magnetic signal consistent with simple collinear AFM order appeared below $T_s \approx 110$ K. Recent x-ray resonant scattering [12] provided direct evidence for charge and concomitant orbital order of the type proposed in [3]. Similar CO/OO was observed in the half-doped pseudocubic manganates [8,9,13]. In both cases, the charge orders at about a twice higher temperature than the spins do, but in the latter, the antiferromagnetic SO is accompanied by a significant lattice distortion and CO/OO quasicommensuration, indicative of their magnetic spin origin. No such effects were seen in the layered $La_{1.5}Sr_{0.5}MnO_4$, where the order is always commensurate and quasi-long-range within the layers. The only hint to the magnetic origin of the CO phase in this case [10] is the smallness of T_c compared to the typical covalent-ordering temperature [3]. In the pure $LaMnO_3$, covalent-bond formation leads to CO/OO at $T_c = 780$ K [4]. The antiferromagnetic SO follows only at $T_N \sim T_c/5$, but causes an appreciable enhancement of the OO, which may also be present in $La_{1.5}Sr_{0.5}MnO_4$ [11].

Here we report a detailed neutron scattering study of the related layered cobalt oxide $La_{1.5}Sr_{0.5}CoO_4$. We argue that strong single-ion anisotropy, mediated by the relativistic spin-orbit coupling usually neglected in cuprates and manganates, effectively decouples charge ordering from low-energy spin fluctuations. This is reflected in the spectacular difference in CO and SO transition temperatures, $T_c/T_s \gtrsim 25$, and absence of any CO anomaly at T_s. Strong planar anisotropy leads to a *quenching of the spin angular momentum* on the Co^{3+} sites, in full analogy with the well-known quenching of the orbital momentum by the crystal field. Combined with the checkerboard arrangement of the holes in CoO_2 planes, this makes the spin system of $La_{1.5}Sr_{0.5}CoO_4$ a strongly frustrated square lattice antiferromagnet.

Electronic configurations of Co^{2+} ($3d^7$) and Co^{3+} ($3d^6$) ions are related to those of Mn^{4+} and Mn^{3+}, respectively, by virtue of electron-hole symmetry. However, in the case of cobalt, Hund's rule is in close competition with the cubic crystal field, the latter splitting the $3d$ level into a lower-lying t_{2g} triplet and an e_g doublet of $d_{x^2-y^2}$ and $d_{3z^2-r^2}$ orbitals. As a result, even though Co^{2+} is in the

high-spin state ($t_{2g}^5 e_g^2$, $S = 3/2$), Co^{3+} obtained by adding the fourth hole may be either in the high $t_{2g}^4 e_g^2$ (HS, $S = 2$), intermediate $t_{2g}^5 e_g^1$ (IS, $S = 1$), or low spin state t_{2g}^6 (LS, $S = 0$) [14]. If LS is the ground state, a decrease in free energy due to the higher spin entropy may drive transitions to IS and HS states with increasing temperature, as observed in $LaCoO_3$ [15]. In our case, however, the spin state of the Co^{3+} ions is not important at sufficiently low temperatures where spin order occurs. Indeed, *any integer spin* will be *frozen in a singlet state* by strong planar anisotropy, rendering ions effectively nonmagnetic for low-energy fluctuations [16].

We studied a piece (0.48 g) of high quality single crystal of $La_{1.5}Sr_{0.5}CoO_4$ grown by the floating-zone method [14]. In the temperature range $6 \lesssim T \lesssim 600$ K covered in our experiment, the crystal remained in the tetragonal "HTT" phase (space group $I4/mmm$), with low T lattice parameters $a = 3.83$ Å and $c = 12.5$ Å. However, to index the superlattice peaks it is convenient to choose a unit cell that is twice as large ($\sqrt{2}\,a \times \sqrt{2}\,a \times c$) corresponding to space group $F4/mmm$.

Experiments were performed on the BT2 and BT4 3-axis thermal neutron spectrometers at the NIST Center for Neutron Research and H8 spectrometer at the High Flux Beam Reactor at Brookhaven. PG(002) reflections were used at the monochromator and analyzer, supplemented by pyrolytic graphite (PG) filters to suppress the higher-order contamination. The energy of the scattered neutrons was fixed at $E_f = 14.7$ meV. Beam collimations before the monochromator and after the analyzer were $\approx 60'$ and $\approx 100'$, respectively, while around the sample they were either $20'-20'$ or $42'-62'$ depending on the required resolution. Our sample is a cylinder with axis parallel to the [010] direction, $D \approx 4$ mm, $L \approx 3$ mm. It was mounted in the displex refrigerator with axis vertical, allowing wave vector transfers in the $(h0l)$ reciprocal lattice plane. Rocking curves about the [010] direction revealed mosaic of less than 0.25°. Normalization of the scattered intensity was done using the incoherent scattering from vanadium.

Figure 1 shows a survey of the low-temperature elastic scattering. Peaks of magnetic and structural origin are easily distinguished by their characteristic wave vector dependences. The magnetic intensity is proportional to the Fourier transform of the density of unpaired electrons (the magnetic form factor) squared, $|f(Q)|^2$, which becomes weaker at large Q, while the intensity from small nuclear displacements increases as $\sim Q^2$. This leads us to conclude that the peaks in Fig. 1(b), centered at slightly incommensurate positions $\boldsymbol{\tau} \pm \mathbf{Q}_m$, $\mathbf{Q}_m = (0.5 + \epsilon, 0, 1)$ with $\epsilon \approx 0.017$, are magnetic, while the strongest peak in Fig. 1(c) and features in Fig. 1(d) result from the atomic displacements accompanying the charge order of Co^{2+}/Co^{3+} ions. None of the superstructure peaks are resolution limited in Q, indicating finite-range *correlated glass*-type modulations. They are static on the time scale $\delta t \lesssim 1$ ps as determined by the energy resolution of our experiment. The

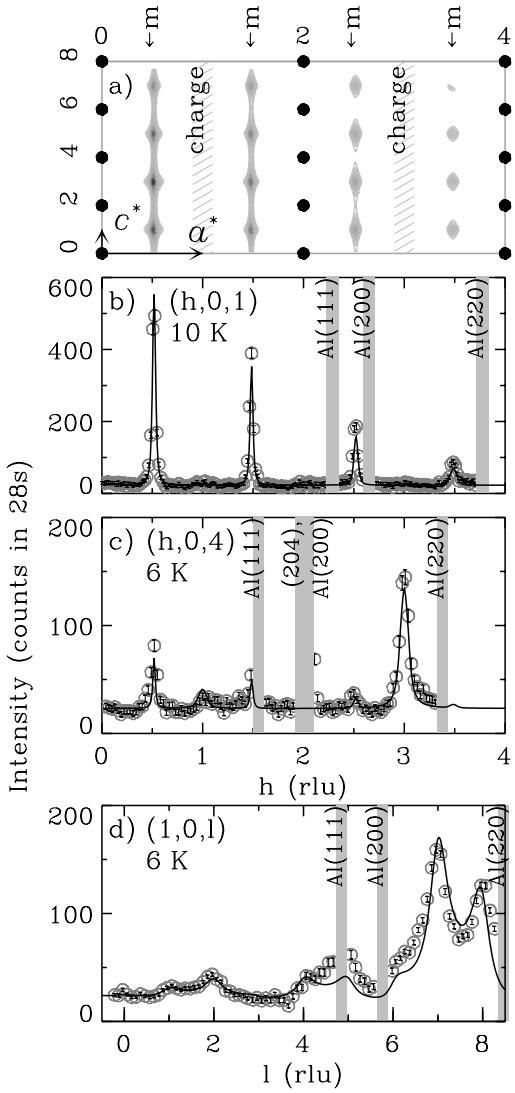

FIG. 1. Survey of the elastic scattering in the $(h0l)$ reciprocal plane of $La_{1.5}Sr_{0.5}CoO_4$. (a) Solid circles show allowed nuclear Bragg reflections; hatched areas mark regions where additional nuclear scattering due to the charge order is observed. The grey-scale map represents calculated magnetic intensity. (b)–(d) Representative scans through the peaks of magnetic and charge-orbital scattering collected at $T = 10$ K (b) and $T = 6.1$ K (c),(d). Points in grey-shaded regions contaminated with aluminum scattering are removed. Solid curves show the fits discussed in the text.

diffuse nature of the scattering is most apparent in scans along the $\mathbf{c}^*$ ([001]) direction, which reflects the anisotropy of the correlation lengths: correlations within the layers are much better developed (see Table I). CO peaks are apparently commensurate, although because of the short correlation length and the overlap of peaks at $\boldsymbol{\tau} \pm \mathbf{Q}_c$, the scattering is also consistent with the modulation wave vectors $\mathbf{Q}_c = (1 + 2\epsilon, 0, l)$ and $(0, 1 + 2\epsilon, l)$, with $l = 0$ or 1. If ϵ is zero, the CO corresponds to a checkerboard arrangement within each CoO_2 plane, shown in Fig. 2(c). The magnetic modulation corresponds to almost antiferromagnetic order on either the Co^{2+} or Co^{3+} sublattice, with a superposed long-wavelength modulation along **a** (or **b**).

TABLE I. Anisotropic correlation lengths of the frozen magnetic and charge-orbital order and approximate positions of the corresponding peaks in reciprocal space.

	$\xi_{\parallel}$ (Å)	$\xi_{\perp}$ (Å)	Peak position
Charge	26(2)	8.1(7)	$\approx(2h \pm 1, 0, l)$
Magnetic	79(3)	10.7(3)	$\approx(2h \pm 0.5, 0, 2l + 1)$

For the quantitative analysis of nuclear scattering accompanying the charge order, we use the following correlation function between the displacement $\boldsymbol{\varepsilon}_{\mu\mathbf{r}}$ of atom μ at position $\mathbf{r} = r_a\hat{\mathbf{a}} + r_b\hat{\mathbf{b}} + r_c\hat{\mathbf{c}}$ and $\boldsymbol{\varepsilon}_{\mu'\mathbf{0}}$ of atom μ' at $\mathbf{0}$:

$$\langle \varepsilon^{\alpha}_{\mu\mathbf{r}} \varepsilon^{\beta}_{\mu'\mathbf{0}} \rangle = \varepsilon^{\alpha}_{\mu} \varepsilon^{\beta}_{\mu'} \cos(\mathbf{Q}_c \mathbf{r}) e^{-(|r_a|+|r_b|)/\xi^{co}_{\parallel} - |r_c|/\xi^{co}_{\perp}}, \quad (1)$$

describing a finite-range harmonic modulation. Brackets denote an average over the crystal volume; $\alpha, \beta = x, y, z$; $\xi^{co}_{\parallel}$ and $\xi^{co}_{\perp}$ are the charge-order correlation lengths parallel and perpendicular to the planes, respectively. The scattering cross section obtained from Eq. (1) upon appropriate Fourier transformation has the form of factorized "lattice Lorentzians" [17] in three directions, weighted with $|\sum_{\mu}(\mathbf{Q} \cdot \boldsymbol{\varepsilon}_{\mu}) b_{\mu} e^{-i\mathbf{Q}\cdot r_{\mu}}|^2$, similar to that used to describe finite-range stripe correlations in LSCO [1]. Here b_{μ} is the scattering length (including the Debye-Waller factor) of the nucleus at position $\mathbf{r}_{\mu}$ in the unit cell. The Q dependence of the structural diffuse intensity evident in scans along $\mathbf{c}^*$, Fig. 1(d), suggests that it arises from breathing-type distortions of the oxygen octahedra surrounding the Co ions. Indeed, it appears sufficient to consider displacements of the in-plane oxygens O(1), $\varepsilon^{x,y}_{O(1)}$, and apical oxygens O(2), $\varepsilon^{z}_{O(2)}$, along the corresponding Co-O bonds, to obtain a good description of the observed "charge" scattering. Solid curves in Figs. 1(c) and 1(d) present the neutron intensity calculated from Eq. (1) after appropriate normalization and correction for the spectrometer resolution. The displacements $\varepsilon^{x,y}_{O(1)} = 0.045(4)$ Å, $\varepsilon^{z}_{O(2)} = -0.071(5)$ Å, and the correlation lengths shown in Table I were obtained in a global fit of all scans around $\boldsymbol{\tau} \pm \mathbf{Q}_c$. The errors above do not include possible systematic error of the vanadium normalization [note the absence of arbitrary scaling between calculated and measured intensities in Figs. 1(a)–1(d)].

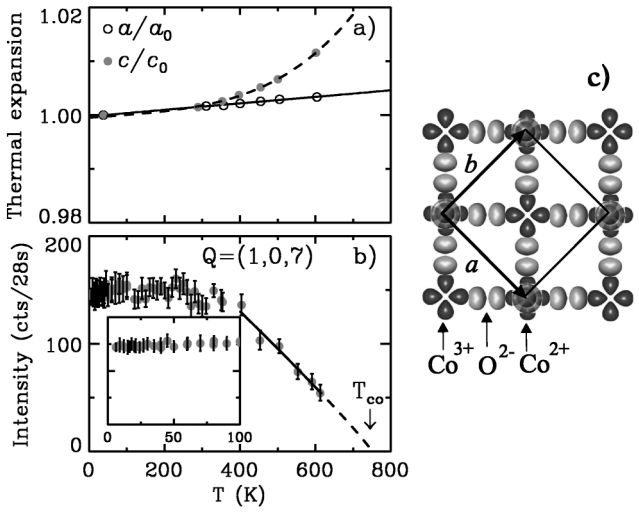

FIG. 2. (a) Relative change in the in-plane (open) and interplane (closed symbols) lattice spacings refined in the longitudinal scans through (200) and (006) Bragg reflections. (b) Temperature dependence of the intensity of the CO diffuse peak at $\mathbf{Q} = (107)$. Inset expands the low-T region, $T \leq 100$ K. (c) Schematic drawing of Co-O bonding orbitals and checkerboard order of Co^{2+}/Co^{3+} valence in the a-b plane.

Figure 2 shows the temperature dependence of the peak intensity of the diffuse CO scattering and lattice thermal expansion in the **a** and **c** directions. Strong nonlinear increase of the c spacing which accompanies melting of the charge order, both starting at ~400 K, is indirect evidence of the concomitant *orbital order*. Indeed, the checkerboard ordering of empty and occupied out-of-plane $d_{3z^2-r^2}$ orbitals, combined with the body-centered stacking of Co-O planes, $\boldsymbol{\delta} = [\frac{1}{2}0\frac{1}{2}]$, allows a reduction of the interplane spacing. Although we could not reach the CO melting temperature, an estimate of $T_c \approx 750$ K is obtained by extrapolation shown in Fig. 2(b).

We analyze the magnetic scattering cross section starting from a spin-spin correlation function similar to Eq. (1). By simultaneously fitting all of the magnetic peaks measured at $T = 10(3)$ K, we obtain a SO incommensurability $\epsilon = 0.017(1)$ and the correlation lengths shown in Table I. We also find that the spin structure is planar, and isotropic within the a-b plane. This agrees with the static susceptibility data [14], which yield an estimated $D \gtrsim 400$ K for the XY-type anisotropy energy. For $T \ll D$ this restricts any integer spin to a singlet state [16]. Further support for the conclusion that Co^{3+} ions are effectively nonmagnetic is provided by a small value of the frozen magnetic moment, $\langle \mu \rangle = 1.4(1)\mu_B$ per Co site refined for a single domain model. Assuming two equivalent $\mathbf{Q}_m$ domains with half of the sites occupied by magnetic Co^{2+} ions, we obtain $\mu_{Co^{2+}} \approx 2.9\mu_B$, within 20% of what is expected for $S = 3/2$.

The main role of the "nonmagnetic" Co^{3+} ions is to bridge the Co^{2+} ions, providing effective antiferromagnetic coupling. As shown in Fig. 2(c), there are two Co^{2+}-O-Co^{3+}-O-Co^{2+} exchange pathways between nearest neighbor (nn) Co^{2+} ions, and one between next-nearest neighbors (nnn). This leads to a simple estimate of the nnn to nn exchange ratio $J_2/J_1 \approx 0.5$. As a result, the spin system appears to be in the critical region where frustration destroys Néel order in a square-lattice antiferromagnet [18]. This provides a natural explanation for the short spin-spin correlation length in the a-b plane and the peculiar *spin freezing* transition revealed by the temperature dependences shown in Fig. 3. Despite a somewhat "order-parameter"-like dependence of the (quasi)elastic magnetic peak intensity, the correlation lengths do not diverge. This is consistent with the spin-glass behavior of the magnetic susceptibility below ~30 K reported in [14]. The defining feature of the transition is the *vanishing of the energy width* Γ_E of the magnetic scattering, i.e.,

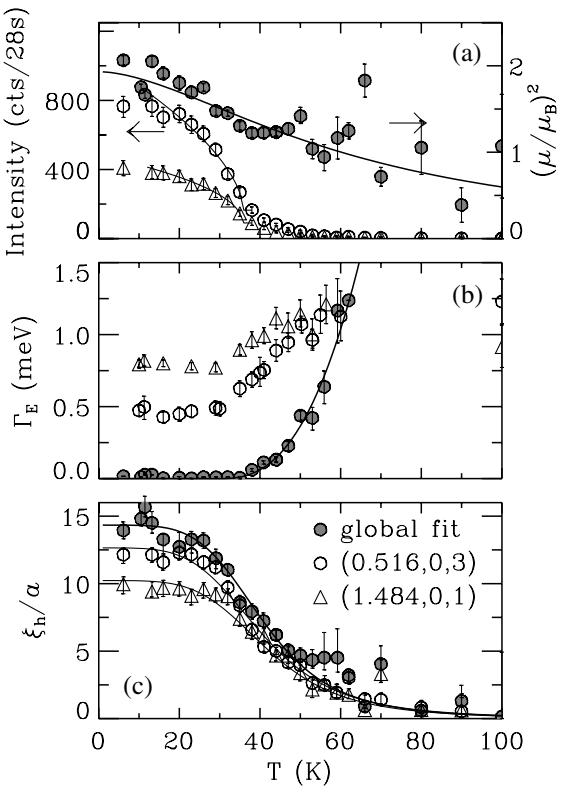

FIG. 3. Temperature dependencies of the SO parameters. Open symbols result from simple fits of the raw data with Lorentzian (a),(c), and Gaussian (b) curves. Shaded circles were obtained from the resolution-corrected global fit of all scans discussed in the text. (a) Peak intensity (left scale) and squared magnetic moment per Co site (right scale), (b) energy width, and (c) the in-plane correlation length. Lines in (a),(c) are guides for the eye.

a divergence of the relaxation time for the spin fluctuations [Fig. 3(b)]. Upon appropriate correction for the instrumental resolution, we are able to refine the $\Gamma_E(T)$ dependence down to $\sim$0.05 meV. From the power-law fit $\Gamma_E(T) \sim (T - T_s)^{\zeta}$ shown in Fig. 3(b) we estimate $\zeta = 2.7(4)$ and $T_s \approx 30$ K. Similar fit to the raw peak intensity in Fig. 3(a) gives slightly higher $T_s \approx 36$ K, characterizing the temperature at which spin fluctuations "enter" our energy resolution window.

To conclude, our results show unambiguously that, in contrast to the half-doped manganates, where CO occurs at low T, and may be driven by spin fluctuations, *charge order in* $La_{1.5}Sr_{0.5}CoO_4$ *is independent of magnetic order*. Not only does it occur at $T_c \gtrsim 25$ times higher than the characteristic energy scale of the cooperative spin fluctuations, it also shows no measurable anomaly at T_s. Compared to the CO in isostructural $La_{1.5}Sr_{0.5}MnO_4$, it has a much shorter correlation range, $\xi_{co}(Mn)/\xi_{co}(Co) \gtrsim 10$, but, surprisingly, results in an even stronger charge localization, with an activation behavior of electrical conductivity with $E_a \sim 6000$ K [14]. Finally, as a result of the checkerboard order of Co^{2+}/Co^{3+} ions and the strong XY anisotropy, the spin system is a stack of weakly interacting square antiferromagnets with nearly critical frustration, $J_2/J_1 \approx 0.5$. In contrast to manganates, where simple collinear AFM order occurs, balancing the double and superexchange, the cobaltate undergoes a freezing transition into a short-range correlated, incommensurate spin-glass state, driven by the frustrated antiferromagnetic superexchange. In fact, it provides a rare example where the evolution of the critical spin fluctuations in the course of glassification can be studied by neutron scattering over a broad dynamic range of several decades.

We thank the NIST Center for Neutron Research for hospitality during the experiments. This work was carried out under Contract No. DE-AC02-98CH10886, Division of Materials Sciences, U.S. Department of Energy.

[1] J. M. Tranquada *et al.,* Phys. Rev. Lett. **78**, 338 (1997); Phys. Rev. B **59**, 14 712 (1999).
[2] V. J. Emery, S. A. Kivelson, and O. Zachar, Phys. Rev. B **56**, 6120 (1997); J. Zaanen, Science **286**, 251 (1999).
[3] J. B. Goodenough, Phys. Rev. B **81**, 564 (1955).
[4] Y. Murakami *et al.,* Phys. Rev. Lett. **81**, 582 (1998).
[5] A. J. Millis, Phys. Rev. B **53**, 8434 (1996).
[6] P. Schiffer, A. P. Ramirez, W. Bao, and S.-W. Cheong, Phys. Rev. Lett. **75**, 3336 (1995).
[7] C. Zener, Phys. Rev. **82**, 403 (1951); P. W. Anderson and H. Hasegawa, Phys. Rev. **100**, 675 (1955).
[8] C.-H. Chen and S.-W. Cheong, Phys. Rev. Lett. **76**, 4042 (1996).
[9] P. G. Radaelli, D. E. Cox, M. Marezio, and S.-W. Cheong, Phys. Rev. B **55**, 3015 (1997).
[10] I. V. Solovyev and K. Terakura, Phys. Rev. Lett. **83**, 2825 (1999); J. van den Brink, G. Khaliullin, and D. Khomskii, Phys. Rev. Lett. **83**, 5118 (1999).
[11] B. J. Sternlieb *et al.,* Phys. Rev. Lett. **76**, 2169 (1996).
[12] Y. Murakami *et al.,* Phys. Rev. Lett. **80**, 1932 (1998).
[13] M. v. Zimmermann *et al.,* Phys. Rev. Lett. **83**, 4872 (1999); Z. Jirák *et al.,* Phys. Rev. B **61**, 1181 (2000).
[14] Y. Moritomo, K. Higashi, K. Matsuda, and A. Nakamura, Phys. Rev. B **55**, R14 725 (1997).
[15] K. Asai *et al.,* J. Phys. Soc. Jpn. **67**, 290 (1998).
[16] A. Abragam and B. Bleaney, *Electron Paramagnetic Resonance of Transition Ions* (Dover, New York, 1986).
[17] M. E. Fisher, Am. J. Phys. **32**, 343 (1964).
[18] M. Zhitomirsky and K. Ueda, Phys. Rev. B **54**, 9007 (1996).